

Thickness-dependent electronic and magnetic properties of γ' -Fe₄N atomic layers on Cu(001)Y. Takahashi,¹ T. Miyamachi,^{1,*} S. Nakashima,¹ N. Kawamura,^{1,2} Y. Takagi,^{3,4} M. Uozumi,^{3,4}
V. N. Antonov,^{5,6} T. Yokoyama,^{3,4} A. Ernst,^{5,7} and F. Komori^{1,†}¹*Institute for Solid State Physics, The University of Tokyo, Kashiwa, Chiba 277-8581, Japan*²*Science and Technology Research Laboratories, NHK, Setagaya, Tokyo 157-8510, Japan*³*Department of Materials Molecular Science, Institute for Molecular Science, Myodaiji-cho, Okazaki 444-8585, Japan*⁴*Department of Structural Molecular Science, The Graduate University for Advanced Studies (SOKENDAI),
Myodaiji-cho, Okazaki 444-8585, Japan*⁵*Max-Planck-Institut für Mikrostrukturphysik, Weinberg 2, 06120 Halle, Germany*⁶*Institute for Metal Physics, 36 Vernadsky Street, 03142 Kiev, Ukraine*⁷*Institut für Theoretische Physik, Johannes Kepler Universität, 4040 Linz, Austria*

(Received 6 February 2017; revised manuscript received 2 May 2017; published 14 June 2017)

Growth, electronic, and magnetic properties of γ' -Fe₄N atomic layers on Cu(001) are studied by scanning tunneling microscopy/spectroscopy and x-ray absorption spectroscopy/magnetic circular dichroism. A continuous film of ordered trilayer γ' -Fe₄N is obtained by Fe deposition under N₂ atmosphere onto monolayer Fe₂N/Cu(001), while the repetition of a bombardment with 0.5 keV N⁺ ions during growth cycles results in imperfect bilayer γ' -Fe₄N. The increase in the sample thickness causes the change in the surface electronic structure, as well as the enhancement in the spin magnetic moment of Fe atoms reaching $\sim 1.4 \mu_B$ /atom in the trilayer sample. The observed thickness-dependent properties of the system are well interpreted by the layer-resolved density of states calculated using first principles, which demonstrates the strongly layer dependent electronic states within each surface, subsurface, and interfacial plane of the γ' -Fe₄N atomic layers on Cu(001).

DOI: [10.1103/PhysRevB.95.224417](https://doi.org/10.1103/PhysRevB.95.224417)**I. INTRODUCTION**

Iron nitrides, especially in iron-rich phases, have been under intense research due to their strong ferromagnetism and interest in its physical origin [1,2]. The difficulty in obtaining a single phase has been a long-standing problem for ferromagnetic iron nitrides, hindering fundamental understanding of intrinsic physical properties [3–5]. Recently, the successful epitaxial growth of single-phase ferromagnetic γ' -Fe₄N has been reported on various substrates, which helps us to comprehend the crucial role of the hybridization between Fe and N states in the ferromagnetism of γ' -Fe₄N [6–12]. The robust Fe-N bonding also renders an Fe₂N layer strongly two-dimensional [13], which possibly facilitates a layer-by-layer stacking of γ' -Fe₄N on metals. This contrasts with the case of elemental 3d transition metals (TMs) deposited on 3d TM substrates, in which inevitable atom intermixing and exchange of constituents prevent the formation of ordered overlayers [14–16]. Therefore, the investigation into the electronic and magnetic states of γ' -Fe₄N atomic layers not only can elucidate the layer-/site-selective electronic and magnetic states of γ' -Fe₄N but also can unravel the origin of the strongly thickness dependent physical properties in a thin-film limit of 3d TM ferromagnets [17–24].

Here, we report two growth modes of γ' -Fe₄N/Cu(001) depending on preparation methods. The scanning tunneling microscopy/spectroscopy (STM/STS) observations indicated a successful growth of ordered trilayer γ' -Fe₄N, without extra nitrogen bombardment onto the existing structures. X-ray absorption spectroscopy/magnetic circular dichroism

(XAS/XMCD) measurements revealed the thickness dependence of the magnetic moments of Fe atoms, the origin of which was well explained by the first-principles calculations. Based on an atomically resolved structural characterization of the system, the layer-by-layer electronic and magnetic states of the γ' -Fe₄N atomic layers have been understood from both experimental and theoretical points of view.

II. METHODS

A clean Cu(001) surface was prepared by repetition of sputtering with Ar⁺ ions and subsequent annealing at 820 K. Iron was deposited at room temperature (RT) in a preparation chamber under an ultrahigh-vacuum (UHV) condition ($< 1.0 \times 10^{-10}$ Torr), using an electron-bombardment-type evaporator (EFM, FOCUS) from a high-purity Fe rod (99.998%). The STM measurements were performed at 77 K in UHV ($< 3.0 \times 10^{-11}$ Torr) using electrochemically etched W tips. The differential conductance dI/dV was recorded for STS using a lock-in technique with a bias-voltage modulation of 20 mV and 719 Hz. The XAS and XMCD measurements were performed at BL 4B of UVSOR-III [25,26] in a total electron yield (TEY) mode. The degree of circular polarization was $\sim 65\%$, and the x-ray propagation vector lay within the (1 $\bar{1}$ 0) plane of a Cu(001) substrate. All the XAS/XMCD spectra were recorded at ~ 8 K, with external magnetic field B up to ± 5 T applied parallel to the incident x ray. The symmetry and quality of the surface were also checked by low-energy electron diffraction (LEED) in each preparation chamber.

First-principles calculations were performed within the density functional theory in the local-density approximation [27], using a self-consistent full-potential Green's function method specially designed for surfaces and interfaces [28,29]. In this approach, a surface or an interface is treated as a

*toshio.miyamachi@issp.u-tokyo.ac.jp

†komori@issp.u-tokyo.ac.jp

layered system with semi-infinite boundary conditions using a so-called surface Green's function method [30], in which layers in the surface or interface vicinity (slab) are matched to the bulk Green's function from one side and to the vacuum or another bulk Green's function from another side. The vacuum potential can be determined by self-consistently solving the corresponding electrostatic problem with proper boundary conditions. In current simulations, we used 16 layers of Cu and 12 layers of vacuum, whose potentials (including Fe and N) were determined self-consistently. We used a 40×40 mesh for two-dimensional Brillouin zone integration and the angular momentum cutoff $l_{\max} = 3$. The energy integration was performed using a contour in the form of a half circle in the complex plane by the Gauss integration method with 32 mesh points. The $3p$ electrons of Cu and Fe were treated as valence electrons. The crystalline structure was not calculated from first principles but adopted from recent experimental studies [31,32] (see the Appendix).

III. RESULTS AND DISCUSSION

A. Monolayer and bilayer-dot γ' -Fe₄N

Monolayer Fe₂N on Cu(001) was prepared prior to any growth of multilayer γ' -Fe₄N by the following cycle: N⁺ ion bombardment with an energy of 0.5 keV to a clean Cu(001) surface, subsequent Fe deposition at RT, and annealing at 600 K. Note that the monolayer Fe₂N is identical to Fe₄N on Cu(001) in a monolayer limit and is thus also referred to as “monolayer γ' -Fe₄N” hereafter. A topographic image of the sample after one growth cycle is shown in Fig. 1(a). The monolayer γ' -Fe₄N is formed on the Cu terraces at ~ 0.85 monolayer (ML) coverage. An atomically resolved image of that surface displayed in Fig. 1(b) reveals a clear dimerization of the Fe atoms, typical of ordered γ' -Fe₄N on Cu(001) [32,33]. A LEED pattern of the surface is shown in Fig. 1(c), which exhibits sharp spots with the corresponding $p4g(2 \times 2)$ symmetry. It is known that [32–35] the topmost layer of the γ' -Fe₄N on Cu(001) always consists of the Fe₂N plane in a bulk Fe₄N crystal shown in Fig. 1(d). A schematic model of the monolayer γ' -Fe₄N is given in Fig. 1(e) and is composed of a single Fe₂N plane on Cu(001). Accordingly, the surface Fe₂N plane takes reconstruction to the $p4g(2 \times 2)$ coordination [33], in which the Fe atoms dimerize in two perpendicular directions, as illustrated in Fig. 1(f).

After repeating the growth cycles, we found a new structure different from the monolayer γ' -Fe₄N. Figure 2(a) displays the surface after two growth cycles in total, namely, another cycle of the N⁺ ion bombardment, Fe deposition, and annealing onto the existing monolayer γ' -Fe₄N surface. Then, the surface becomes mostly covered with the monolayer γ' -Fe₄N, which contains a small number of bright dots. For structural identification of these dots, we measured atomically resolved topographic images and line profiles at different V_s , as shown in Figs. 2(b) and 2(c). The dot structure imaged at $V_s = -0.1$ V reveals the dimerization of the Fe atoms as the monolayer γ' -Fe₄N surface. This indicates that the topmost part of the dot consists of the reconstructed Fe₂N. At positive V_s of +0.1 V, in contrast, the dot is recognized as a single protrusion in both the topographic image and line profile, while the surrounding

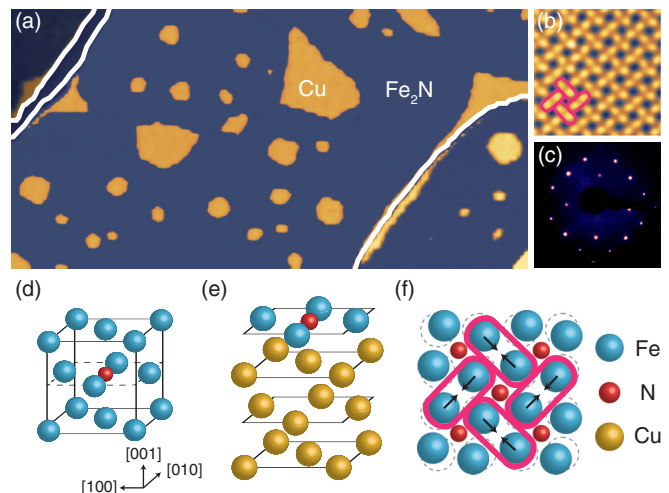


FIG. 1. Topography and atomic structure of the monolayer γ' -Fe₄N on Cu(001). (a) Topographic image (100×50 nm², sample bias $V_s = +1.0$ V, tunneling current $I = 0.1$ nA) of the monolayer γ' -Fe₄N on Cu(001). White lines represent step edges of the Cu(001) terraces. Color contrast is enhanced within each terrace. (b) Close view (2.5×2.5 nm², $V_s = 0.25$ V, $I = 45$ nA) of the surface Fe₂N layer. The dimerization of Fe atoms is indicated by encirclement. (c) LEED pattern obtained with an incident electron energy of 100 eV. (d) Bulk crystal structure of γ' -Fe₄N. A dotted parallelogram represents an Fe₂N plane. (e) Atomic structure of the monolayer γ' -Fe₄N on Cu(001). (f) Schema illustrating $p4g(2 \times 2)$ reconstruction in the surface Fe₂N layer of γ' -Fe₄N. Arrows indicate the shift of the Fe atoms from an unreconstructed $c(2 \times 2)$ coordination (dotted circles). For (d) to (f), large blue (yellow) and small red spheres represent Fe (Cu) and N atoms, respectively.

monolayer γ' -Fe₄N still shows the Fe dimerization. This implies the different electronic structure of the dot compared to that of the monolayer γ' -Fe₄N, which comes from the difference in a subsurface atomic structure.

The observed height difference between the dot and the monolayer γ' -Fe₄N ranges from 4 to 10 pm depending on V_s . These values are on the same order as a lattice mismatch between the bulk crystals of the γ' -Fe₄N/Cu(001) (380 pm) and Cu(001) (362 pm) [33] but an order of magnitude smaller than the lattice constant of the γ' -Fe₄N/Cu(001). This suggests that the topmost layer of the dot is not located above the monolayer γ' -Fe₄N but shares the Fe₂N plane with the surrounding surface. Furthermore, the bright dot is composed of only four pairs of the Fe dimer, as shown in Fig. 2(b), indicating that the difference in the atomic and/or electronic structures is restricted within a small area.

The STS observations attributed the bias dependence of the topographic images mainly to the variation in electronic structures. Figure 2(d) presents dI/dV spectra recorded on the dot and monolayer surface. While a small difference between the spectra can be recognized on a negative V_s side, the peak intensity considerably differs at positive V_s below +1.0 V, where the Fe and N states strongly hybridize each other [32]. This implies that the dot contains another Fe atom interacting with the N atom, electronically different from those in the topmost layer. Considering all the above, it is most plausible that one Fe atom is embedded just under the surface N atom

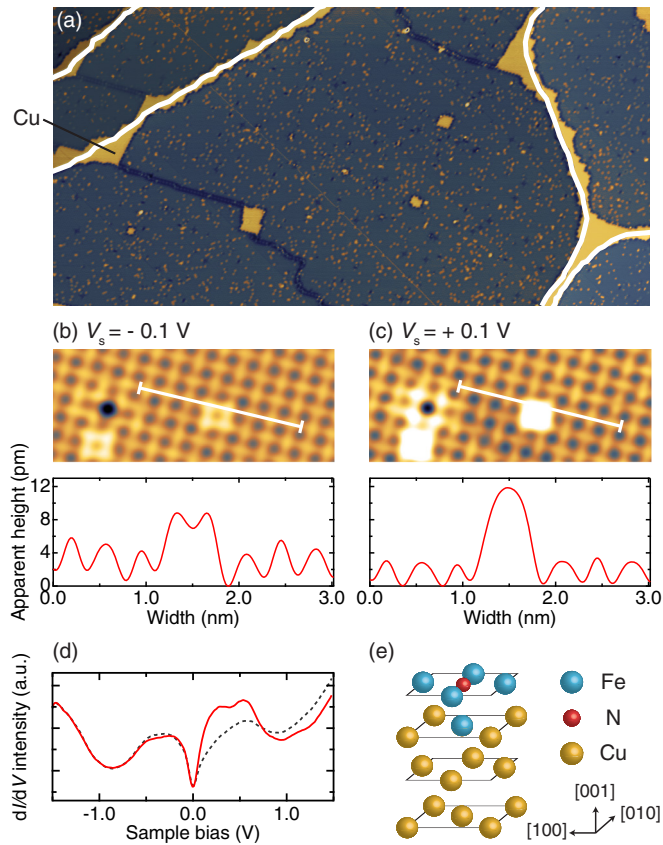


FIG. 2. Topography of the bilayer γ' -Fe₄N dot on Cu(001). (a) Topographic image ($120 \times 60 \text{ nm}^2$, $V_s = -0.1 \text{ V}$, $I = 0.1 \text{ nA}$) of the monolayer (darker area) and dotlike bilayer γ' -Fe₄N on Cu(001). White lines represent step edges of the Cu(001) terraces. Color contrast is enhanced within each terrace. (b) and (c) Top: Atomically resolved topographic images ($7 \times 2 \text{ nm}^2$, $I = 2.0 \text{ nA}$) taken at (b) $V_s = -0.1 \text{ V}$ and (c) $+0.1 \text{ V}$. Bottom: Height profiles measured along lines indicated in the top panels. (d) Experimental dI/dV spectra recorded atop the bright dot (solid line) and the monolayer surface (dotted line). The dI/dV intensity is arbitrary, and a STM tip was stabilized at $V_s = -1.5 \text{ V}$, $I = 3.0 \text{ nA}$. (e) Proposed atomic structure of the bilayer-dot γ' -Fe₄N on Cu(001). Large blue (yellow) and small red spheres correspond to Fe (Cu) and N atoms, respectively.

at the dot center, and thus, a bilayer γ' -Fe₄N dot is formed, as schematically shown in Fig. 2(e). This structure corresponds to a minimum unit of the bilayer γ' -Fe₄N on Cu(001).

This bilayer dot formed clusters by a further repetition of the growth cycles. Figure 3(a) shows an enlarged view of the iron nitride surface after two growth cycles. The coverage of the dot is estimated to be $\sim 5\%$ of the entire surface. Another growth cycle onto this surface led to an increase in dot density up to $\sim 40\%$, as shown in Fig. 3(b). However, further repetitions of the cycles resulted in neither a considerable increase in the dot density nor the formation of a continuous bilayer film. This can be attributed to an inevitable sputtering effect in every growth cycle: an additional N^+ ion bombardment to the existing surface not only implanted N^+ ions but also sputtered the surface, which caused the loss of the iron nitrides already formed at the surface, as well as the increase in the surface roughness.

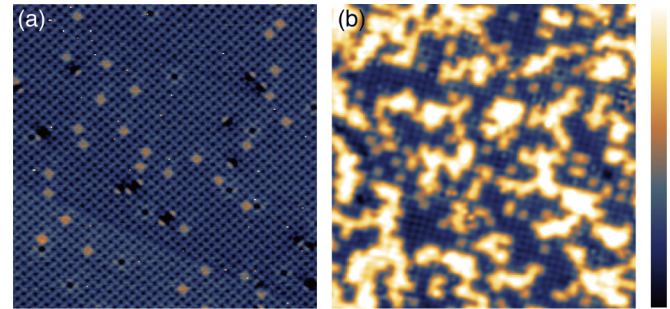


FIG. 3. Topographic images ($15 \times 15 \text{ nm}^2$) of the surface after repetition of (a) two and (b) three growth cycles. The set point is $(V_s, I) = (+0.25 \text{ V}, 5.0 \text{ nA})$ for (a) and $(+0.1 \text{ V}, 3.0 \text{ nA})$ for (b).

To compensate this loss of surface Fe atoms by the sputtering effect, we also tried to increase the amount of deposited Fe per cycle. Nonetheless, the number of Fe atoms, which remained at the surface after annealing, did not increase, possibly because of the thermal metastability of Fe/Cu systems [36–39]. The isolated Fe atoms without any bonding to N atoms were easily diffused and embedded into the Cu substrate during the annealing process. As a result, only the imperfect bilayer γ' -Fe₄N was obtained through this method.

B. Trilayer γ' -Fe₄N film

Multilayer γ' -Fe₄N films were obtained by the following procedure. First, the monolayer γ' -Fe₄N was prepared on Cu(001) as above. Then, 2-ML Fe was deposited under a N_2 atmosphere ($5.0 \times 10^{-8} \text{ Torr}$) [40] at RT, and the sample was annealed at 600 K. Figures 4(a) and 4(b) show topographic images after two and three such cycles, respectively. In the images, the coverage of a new bright area, different from the imperfect bilayer dot, monotonously increases with repeating the cycles. A close view of that new surface is displayed in Fig. 4(c), revealing the dimerized [or even $c(2 \times 2)$ -like dot] structures. Because a LEED pattern shown in the inset of Fig. 4(c) exhibits the $p4g(2 \times 2)$ symmetry without extra spots, the topmost layer of this surface is composed of the reconstructed Fe₂N plane [32]. Therefore, these observations suggest that the new area would consist of γ' -Fe₄N other than both the monolayer and bilayer dot.

In order to determine the structure of this newly obtained γ' -Fe₄N, a typical height profile of the surface was recorded, as shown in Fig. 4(d). It is clear that the new structure is higher than both the Cu surface and the surface including the monolayer/dotlike bilayer γ' -Fe₄N. This suggests that the new area is composed of γ' -Fe₄N thicker than bilayer. Quantitative information on the thickness of the new structure could be obtained from Fe $L(2p \rightarrow 3d)$ edge jump spectra shown in Fig. 4(e), whose intensity is roughly proportional to the number of surface/subsurface Fe atoms. The sample prepared in the same procedure as that shown in Fig. 4(b) reveals an edge jump value of 0.32, while the monolayer γ' -Fe₄N has a value of 0.12 [41]. Considering that the new area occupies $\sim 60\%$ of the entire surface, as deduced from Fig. 4(b), the thickness of this γ' -Fe₄N must be less than quadlayer to meet the experimental edge jump value of 0.32. Hence, the newly obtained structure is identified as a trilayer γ' -Fe₄N

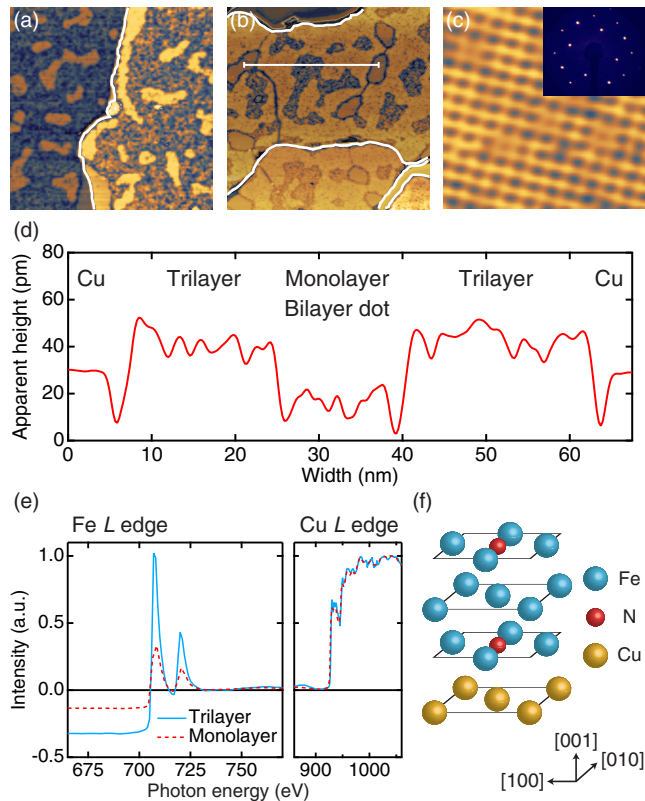


FIG. 4. Topography of the trilayer γ' -Fe₄N film on Cu(001). Topographic images ($100 \times 100 \text{ nm}^2$) after (a) two and (b) three cycles of the Fe deposition under N₂ atmosphere and subsequent annealing onto the monolayer γ' -Fe₄N on Cu(001). The set point is $I = 0.1 \text{ nA}$ and $V_s = -0.1 \text{ V}$ for (a) and -0.05 V for (b). White lines indicate step edges of the Cu terraces. Color contrast is enhanced within each terrace. (c) Atomically resolved topographic image ($4 \times 4 \text{ nm}^2$, $I = 5.0 \text{ nA}$, $V_s = -0.1 \text{ V}$) of the trilayer γ' -Fe₄N surface. The inset represents a LEED pattern of the sample shown in (b), obtained with an incident electron energy of 100 eV . (d) Height profile measured along the line indicated in (b). (e) XAS edge jump spectra of the trilayer (solid line) and monolayer (dotted line) samples at the Fe and Cu L edges. The intensity is normalized to the Cu edge jump. (f) Atomic model expected for the trilayer γ' -Fe₄N on Cu(001). Blue (yellow) large and red small spheres represent Fe (Cu) and N atoms, respectively.

film. An atomic structure expected for the trilayer γ' -Fe₄N on Cu(001) is presented in Fig. 4(f). The growth without any ion bombardment to the monolayer surface possibly stabilizes the subsurface pure Fe layer, which could promote the formation of the trilayer γ' -Fe₄N film in a large area.

Finally, let us mention another growth method of the γ' -Fe₄N film. We previously reported a possible layer-by-layer growth of the γ' -Fe₄N atomic layers on Cu(001) by the N⁺ ion bombardment with a relatively low energy of 0.15 keV [31]. This soft implantation of N⁺ ions successfully avoids extra damage to the existing γ' -Fe₄N structures during the repetition of the growth cycles. The reported different electronic/magnetic states could then originate from the difference in the fabrication processes. Another finding is that, in the current study, only the monolayer and trilayer γ' -Fe₄N could be obtained in a continuous film form. This implies that

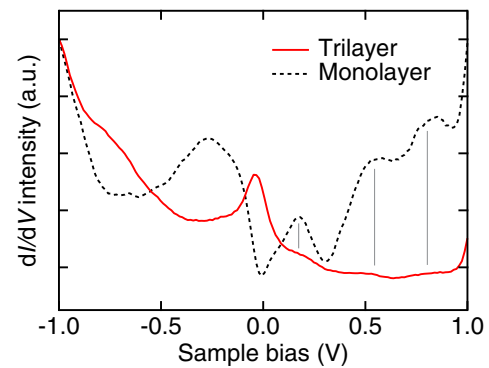


FIG. 5. Surface electronic structures of the γ' -Fe₄N on Cu(001). Experimental dI/dV spectra recorded above the trilayer (solid line) and monolayer (dotted line) γ' -Fe₄N surfaces are presented. The dI/dV intensity is arbitrary. A STM tip was stabilized at $V_s = +1.0 \text{ V}$ and $I = 3.0 \text{ nA}$. Gray lines are a guide to the eye.

an Fe₂N-layer termination would be preferable through the present methods, as proposed in the previous theoretical study [42].

C. Electronic and magnetic properties of γ' -Fe₄N atomic layers

The surface electronic structures of γ' -Fe₄N showed a large dependence on the sample thickness. Figure 5 displays experimental dI/dV spectra measured on the surfaces of the trilayer and monolayer γ' -Fe₄N. The peaks located at $V_s \sim +0.20$, $+0.55$, and $+0.80 \text{ V}$, mainly originating from the unoccupied states in the down-spin band characteristic of the Fe local density of states (LDOS), are observed for both the trilayer and monolayer surfaces [43]. A significant difference between the spectra is a dominant peak located around $V_s = -50 \text{ mV}$ observed only for the trilayer surface. This peak possibly originates from the LDOS peak located around $E - E_F = -0.2 \text{ eV}$, calculated for the Fe atoms not bonded to N atoms in the subsurface Fe layer [corresponding site of Fe4 shown in Fig. 7(a) below]. Because the $d_{3z^2-r^2}$ orbital extends toward the vacuum side, this peak could be dominantly detected in the STS spectrum for the trilayer surface. Thus, the appearance of this additional peak could support the different subsurface structure of the trilayer sample, especially the existence of the subsurface Fe layer proposed above.

All electronic and magnetic properties of the sample, including both surface and subsurface information, were investigated by using XAS and XMCD techniques at the Fe $L_{2,3}$ ($2p_{1/2,3/2} \rightarrow 3d$) absorption edges. Figure 6(a) shows XAS (μ_+ , μ_-) and XMCD ($\mu_+ - \mu_-$) spectra under $B = \pm 5 \text{ T}$ for the trilayer and monolayer samples in the grazing ($\theta = 55^\circ$) and normal incidences ($\theta = 0^\circ$). Here, μ_+ (μ_-) denotes an x-ray absorption spectrum with the photon helicity parallel (antiparallel) to the Fe $3d$ majority spin, and an incident angle θ is defined as that between the sample normal and incident x rays. The trilayer (monolayer) sample was prepared using the same procedure as that shown in Fig. 4(b) [Fig. 1(a)]. It is clear that the XMCD intensity is larger in the trilayer one, indicating an enhancement of magnetic moments with increasing thickness.

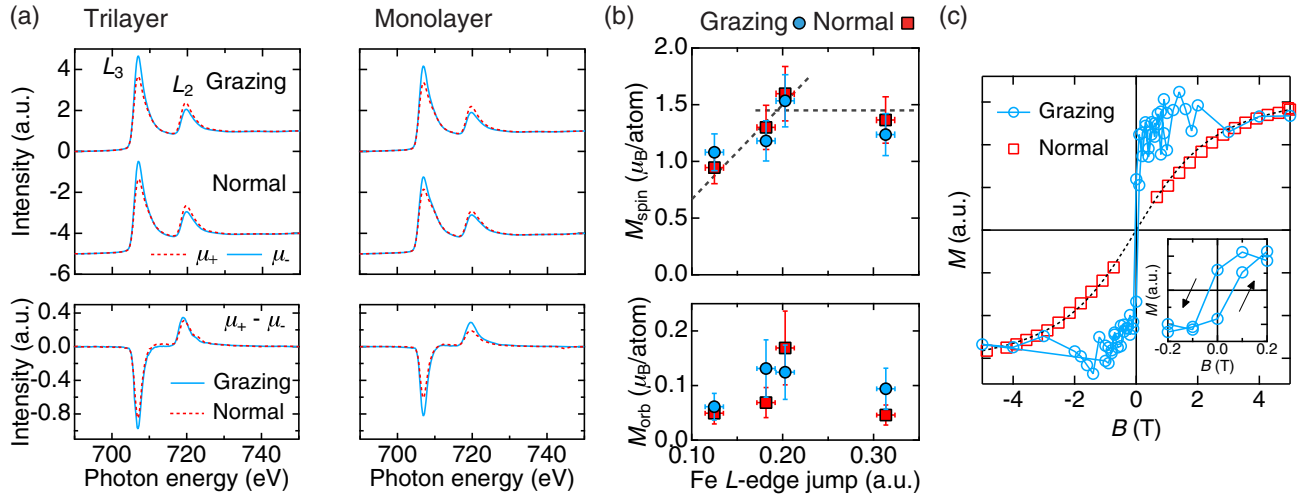


FIG. 6. Thickness-dependent electronic and magnetic properties of the γ' -Fe₄N atomic layers on Cu(001). (a) Top: XAS spectra under $B = \pm 5$ T of the trilayer (left) and monolayer (right) samples in the grazing (top lines) and normal (bottom lines) incidence. Bottom: Corresponding XMCD spectra in the grazing (solid line) and normal (dotted line) incidence. All the spectra are normalized to the Fe XAS L -edge jump. (b) Top (bottom): Experimental spin (orbital) magnetic moment in the grazing (circles) and normal (squares) incidences plotted with respect to the Fe L -edge jump values. The edge jump values of 0.12 and 0.32 correspond to those of the monolayer and trilayer samples, respectively. Dotted lines are a guide to the eye. Error bars are indicated for all the data and are smaller than the symbol size if not seen. (c) Magnetization of the monolayer sample recorded in the grazing (circles and solid line) and normal (squares) incidences. The dotted line is a guide to the eye. The inset shows an enlarged view of the curve recorded in the grazing incidence.

For a further quantitative analysis of the magnetic moments, we applied XMCD sum rules [44,45] to the obtained spectra and estimated spin (M_{spin}) and orbital (M_{orb}) magnetic moments separately. Note that the average number of $3d$ holes n_{hole} of 3.2 was used in the sum-rule analysis, which was estimated by comparing the area of the experimental XAS spectra with that of a reference spectrum of bcc Fe/Cu(001) ($n_{\text{hole}} = 3.4$) [46]. The thickness dependence of the M_{spin} and M_{orb} values is summarized in Fig. 6(b). The value of M_{spin} increases monotonously with increasing the Fe L -edge jump value, namely, an average sample thickness, and finally saturates at $\sim 1.4 \mu_B/\text{atom}$ in the trilayer sample (corresponding edge jump value of 0.32). The change in M_{orb} is not so systematic relative to M_{spin} ; however, the M_{orb} values seem to be enhanced in the grazing incidence. This implies an in-plane easy magnetization of the γ' -Fe₄N atomic layers on Cu(001), also consistent with the previous reports on the γ' -Fe₄N thin films on Cu(001) [8,31]. Figure 6(c) shows magnetization curves of the monolayer sample, whose intensity corresponds to the L_3 -peak XAS intensity normalized to the L_2 one. The curve recorded in the normal incidence shows negligible remanent magnetization. On the other hand, that in the grazing one draws a rectangular hysteresis loop, which confirms the in-plane easy magnetization. The coercivity of the monolayer sample is estimated to be ~ 0.05 T at 8.0 K, larger than ~ 0.01 T for 5-ML Fe/Cu(001) [21], ~ 1 mT for 5-ML Fe/GaAs(100)-(4 × 6) [47], and the 30-nm-thick γ' -Fe₄N film [8] at RT.

D. Theoretical analysis of the electronic and magnetic states of γ' -Fe₄N atomic layers on Cu(001)

The observed thickness dependence of the magnetic moments can be well understood with the help of first-principles calculations. Based on structural models presented in Fig. 7(a),

the layer-resolved DOS of the monolayer and trilayer γ' -Fe₄N on Cu(001) was obtained as shown in Figs. 7(b) and 7(c), respectively [48]. In Table I, calculated values of M_{spin} and M_{orb} along the easy magnetization direction are also listed for each Fe site. In the monolayer case, the calculated M_{spin} is $1.1 \mu_B/\text{atom}$, which is in perfect agreement with the experimental value. This supports the ideal atomic structure of our monolayer sample.

Interestingly, the value of M_{spin} for the Fe atoms in the monolayer γ' -Fe₄N is more than 1.5 times smaller than that in the topmost layer of the trilayer one ($1.83 \mu_B/\text{atom}$, Fe1 and Fe2). In comparison with the DOS shown at the top of Fig. 7(c), the impact of the hybridization with the Cu states on the Fe DOS can be seen in Fig. 7(b): First, the DOS in the up-spin band, especially with $d_{3z^2-r^2}$ and d_{yz} orbitals, begins to have a tail toward the higher-energy side across E_F . This change causes the $3d$ electrons in the up-spin band to deviate from a fully occupied nature. Moreover, the spin asymmetry of the occupied $3d$ electrons, the difference between the electron occupation in each spin band normalized by their sum, decreases, especially for the DOS with d_{xy} , $d_{3z^2-r^2}$, and d_{yz} orbitals. These changes could decrease M_{spin} of the Fe atoms. Note that a similar reduction in the magnetic moments of $3d$ TMs due to the hybridization with Cu states is reported, for example, in Refs. [49,50].

Then, by comparing two different Fe₂N interfaces with the Cu substrate, it turns out that M_{spin} of the monolayer γ' -Fe₄N ($1.1 \mu_B/\text{atom}$) is almost twice that of the trilayer one ($0.62 \mu_B/\text{atom}$, Fe5 and Fe6). In the monolayer case, the Fe₂N layer faces a vacuum, and the Fe atoms are under reduced atomic coordination. This results in the narrower bandwidth, and thus, the DOS intensity increases in the vicinity of E_F . Accordingly, a larger exchange splitting could be possible, and the spin asymmetry of the occupied $3d$ electrons increases

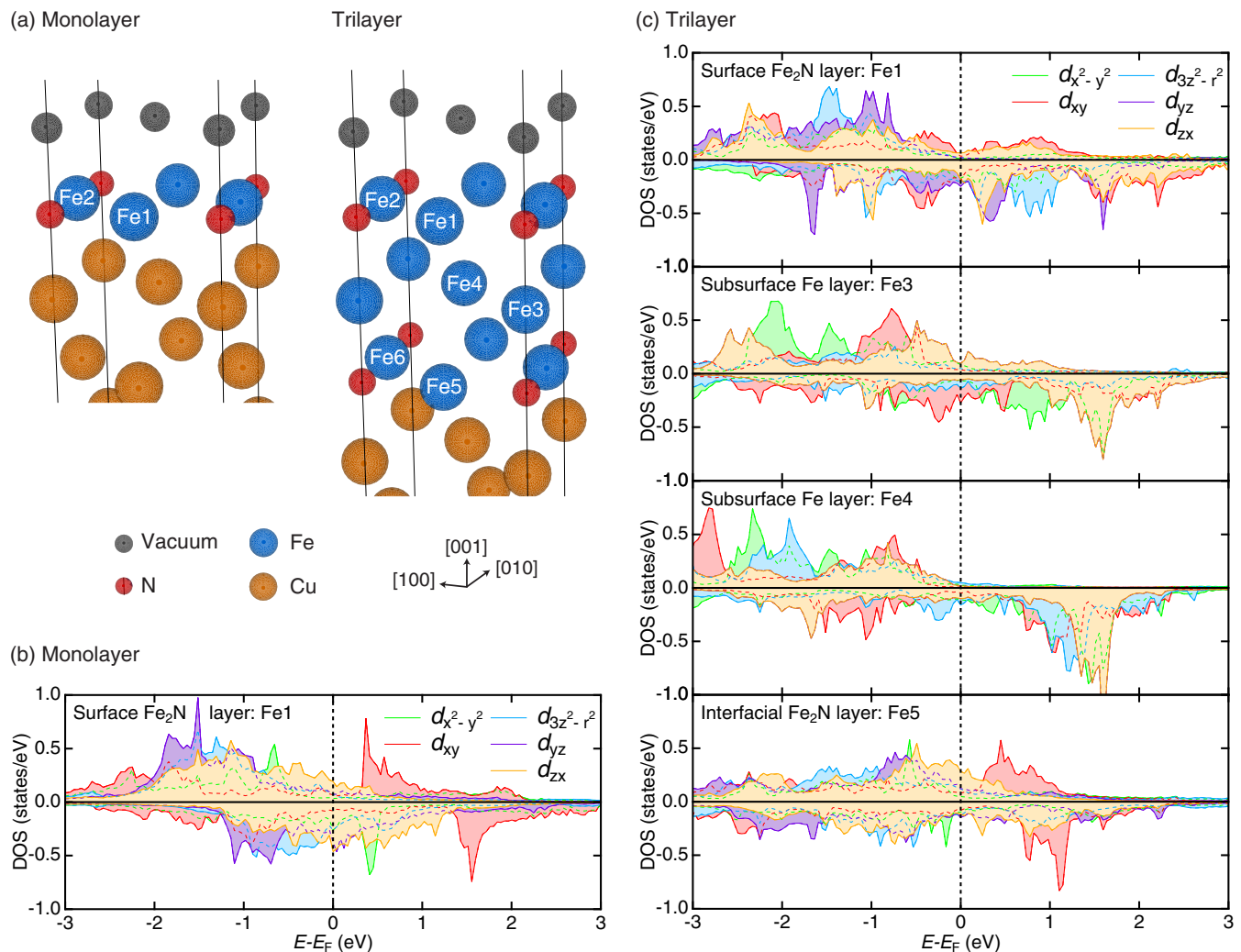


FIG. 7. Layer-by-layer electronic states of the γ' -Fe₄N atomic layers on Cu(001). (a) Site notation of Fe atoms indicated for pristine $c(2 \times 2)$ crystal structures of monolayer (left) and trilayer (right) γ' -Fe₄N. Black, red, blue, and yellow spheres represent vacuum and N, Fe, and Cu atoms, respectively. (b) and (c) Calculated layer-resolved DOS projected to each 3d orbital of the (b) monolayer and (c) trilayer γ' -Fe₄N on Cu(001). The DOS in the up-spin (down-spin) band is shown in the top (bottom) panels. Note that the states with d_{yz} and d_{zx} orbitals are degenerated for the Fe3 and Fe4 sites in (c).

as shown in Fig. 7(b) compared to the interfacial Fe₂N layer of the trilayer γ' -Fe₄N [bottom panel of Fig. 7(c)]. This leads to larger magnetic moments at the surface. As a result, the competition between the enhancement at the surface and the decrease at the interface would make M_{spin} values quite layer sensitive.

TABLE I. Calculated values of M_{spin} (top values) and M_{orb} (bottom values) for the Fe atoms at each site (in units of μ_B/atom). The site notation is the same as that used in Fig. 7.

	Surface Fe ₂ N		Subsurface Fe		Interfacial Fe ₂ N	
	Fe1	Fe2	Fe3	Fe4	Fe5	Fe6
Monolayer	1.1	1.1				
	0.027	0.027				
Trilayer	1.8	1.8	2.0	3.0	0.62	0.62
	0.023	0.023	0.005	0.007	0.016	0.016

In the subsurface Fe layer of the trilayer γ' -Fe₄N (Fe3 and Fe4), the value of M_{spin} becomes largest due to the bulk coordination of the Fe atoms. Especially, the Fe atoms not bonded to N atoms (Fe4) possess M_{spin} of 3.0 μ_B/atom , which is comparable to the values of Fe atoms at the same site in the bulk γ' -Fe₄N [2]. Consequently, by averaging the layer-by-layer M_{spin} values of the trilayer γ' -Fe₄N, the total magnetic moment detected in the XMCD measurement is expected to be 1.7 μ_B/Fe , with an electron escape depth of 17 Å reported for Fe thin films taken into account [51]. Considering the composition expected for the trilayer sample, this value can well explain the experimental one of $\sim 1.5 \mu_B/\text{Fe}$ atom.

The theory also demonstrates the direction of an easy magnetization axis. The in-plane easy magnetization of our γ' -Fe₄N samples was confirmed by the magnetization curves as well as the incidence dependence of the M_{orb} value. In contrast, the pristine ultrathin Fe films, which form either fct or fcc structures on Cu(001), show uncompensated out-of-plane spins over a few surface layers [24,52]. This shift of magnetic

anisotropy by nitridation can be understood from the orbital-resolved Fe DOS shown in Figs. 7(b) and 7(c). Unlike the pure Fe/Cu(001) system [53], the occupation of 3d electrons in states with out-of-plane-oriented orbitals (d_{yz} , d_{zx} , $d_{3z^2-r^2}$) is considerably larger than that with in-plane-oriented ones (d_{xy} , $d_{x^2-y^2}$). This could make M_{orb} prefer to align within a film plane, resulting in the in-plane magnetization of the system [54].

IV. SUMMARY

In conclusion, we have conducted a detailed study of the growth, electronic, and magnetic properties of the γ' -Fe₄N atomic layers on Cu(001). The ordered trilayer film of γ' -Fe₄N can be prepared by Fe deposition under N₂ atmosphere onto the existing monolayer surface. On the other hand, repetition of the growth cycles including the high-energy N⁺ ion implantation resulted in the imperfect bilayer γ' -Fe₄N. The STM and STS observations revealed the change in the surface topography and electronic structures with increasing sample thickness. The XAS and XMCD measurements also showed the thickness dependence of the spectra and the corresponding evolution of the M_{spin} values. All the thickness dependence of the electronic and magnetic properties is well explained by the layer-resolved DOS calculated using first principles. Structural perfection of the system makes it possible to fully comprehend the layer-by-layer electronic/magnetic states of the γ' -Fe₄N atomic layers.

ACKNOWLEDGMENTS

This work was partly supported by the JSPS Grant-in-Aid for Young Scientists (A) (Grant No. 16H05963), for

TABLE II. Atomic positions used in the first-principles calculations for the monolayer and trilayer γ' -Fe₄N. The x , y , and z coordinates (in Å) are taken along the [100], [010], and [001] crystal axes, respectively.

	Atom	Monolayer			Trilayer		
		x	y	z	x	y	z
Surface	N	0	0	0.23	0	0	0.27
	N	3.62	0	-0.24	3.62	0	-0.04
	Fe	1.81	0.39	0.05	1.85	0.26	0.05
Subsurface	Fe				0	0	-1.76
	Fe				3.62	0	-1.85
Interface	N				0	0	-3.39
	N				3.62	0	-3.86
	Fe				1.81	0.39	-3.57

Scientific Research (B) (Grant No. 26287061), the Hosono Foundation, the Shimadzu Science Foundation, the Iketani Science and Technology Foundation, and the Nanotechnology Platform Program (Molecule and Material Synthesis) of the Ministry of Education, Culture, Sports, Science and Technology (MEXT), Japan. Y.T. was supported by a Grant-in-Aid for JSPS Fellows and the Program for Leading Graduate Schools (MERIT). A.E. acknowledges funding from the German Research Foundation (DFG Grant No. ER 340/4-1).

APPENDIX: ATOMIC POSITIONS OF THE THEORETICAL STRUCTURAL MODEL

Crystal structures used in the first-principles calculations are summarized in Table II. The minimum required number of atomic coordinates is presented for each layer. Note that the positions of Cu atoms are not shifted with respect to the pristine fcc lattice of Cu(001).

-
- [1] J. Coey and P. Smith, *J. Magn. Magn. Mater.* **200**, 405 (1999).
 - [2] B. C. Frazer, *Phys. Rev.* **112**, 751 (1958).
 - [3] J. M. D. Coey, *J. Appl. Phys.* **76**, 6632 (1994).
 - [4] M. Komuro, Y. Kozono, M. Hanazono, and Y. Sugita, *J. Appl. Phys.* **67**, 5126 (1990).
 - [5] C. Ortiz, G. Dumpich, and A. H. Morrish, *Appl. Phys. Lett.* **65**, 2737 (1994).
 - [6] S. Atiq, H.-S. Ko, S. A. Siddiqi, and S.-C. Shin, *Appl. Phys. Lett.* **92**, 222507 (2008).
 - [7] D. M. Borsa, S. Grachev, D. O. Boerma, and J. W. J. Kerssemakers, *Appl. Phys. Lett.* **79**, 994 (2001).
 - [8] J. M. Gallego, S. Y. Grachev, D. M. Borsa, D. O. Boerma, D. Écija, and R. Miranda, *Phys. Rev. B* **70**, 115417 (2004).
 - [9] K. Ito, G. H. Lee, K. Harada, M. Suzuno, T. Suemasu, Y. Takeda, Y. Saitoh, M. Ye, A. Kimura, and H. Akinaga, *Appl. Phys. Lett.* **98**, 102507 (2011).
 - [10] K. R. Nikolaev, I. N. Krivorotov, E. D. Dahlberg, V. A. Vas'ko, S. Urazhdin, R. Loloee, and W. P. Pratt, *Appl. Phys. Lett.* **82**, 4534 (2003).
 - [11] S. Kokado, N. Fujima, K. Harigaya, H. Shimizu, and A. Sakuma, *Phys. Rev. B* **73**, 172410 (2006).
 - [12] K. Ito, K. Toko, Y. Takeda, Y. Saitoh, T. Oguchi, T. Suemasu, and A. Kimura, *J. Appl. Phys.* **117**, 193906 (2015).
 - [13] C.-M. Fang, R. S. Koster, W.-F. Li, and M. A. van Huis, *RSC Adv.* **4**, 7885 (2014).
 - [14] S. H. Kim, K. S. Lee, H. G. Min, J. Seo, S. C. Hong, T. H. Rho, and J.-S. Kim, *Phys. Rev. B* **55**, 7904 (1997).
 - [15] F. Nouvertné, U. May, M. Bamming, A. Rampe, U. Korte, G. Güntherodt, R. Pentcheva, and M. Scheffler, *Phys. Rev. B* **60**, 14382 (1999).
 - [16] P. Torelli, F. Sirotti, and P. Ballone, *Phys. Rev. B* **68**, 205413 (2003).
 - [17] P. Srivastava, N. Haack, H. Wende, R. Chauvistré, and K. Baberschke, *Phys. Rev. B* **56**, R4398 (1997).
 - [18] M. Farle, W. Platow, A. N. Anisimov, P. Pouloupoulos, and K. Baberschke, *Phys. Rev. B* **56**, 5100 (1997).
 - [19] M. Farle, B. Mirwald-Schulz, A. N. Anisimov, W. Platow, and K. Baberschke, *Phys. Rev. B* **55**, 3708 (1997).
 - [20] B. Schulz and K. Baberschke, *Phys. Rev. B* **50**, 13467 (1994).
 - [21] D. Li, M. Freitag, J. Pearson, Z. Q. Qiu, and S. D. Bader, *Phys. Rev. Lett.* **72**, 3112 (1994).

- [22] M. Straub, R. Vollmer, and J. Kirschner, *Phys. Rev. Lett.* **77**, 743 (1996).
- [23] W. Weber, A. Bischof, R. Allenspach, C. H. Back, J. Fassbender, U. May, B. Schirmer, R. M. Jungblut, G. Güntherodt, and B. Hillebrands, *Phys. Rev. B* **54**, 4075 (1996).
- [24] H. L. Meyerheim, J.-M. Tonnerre, L. Sandratskii, H. C. N. Tolentino, M. Przybylski, Y. Gabi, F. Yildiz, X. L. Fu, E. Bontempi, S. Grenier, and J. Kirschner, *Phys. Rev. Lett.* **103**, 267202 (2009).
- [25] T. Gejo, Y. Takata, T. Hatsui, M. Nagasono, H. Oji, N. Kosugi, and E. Shigemasa, *Chem. Phys.* **289**, 15 (2003).
- [26] T. Nakagawa, Y. Takagi, Y. Matsumoto, and T. Yokoyama, *Jpn. J. Appl. Phys.* **47**, 2132 (2008).
- [27] J. P. Perdew and Y. Wang, *Phys. Rev. B* **45**, 13244 (1992).
- [28] M. Lüders, A. Ernst, W. M. Temmerman, Z. Szotek, and P. J. Durham, *J. Phys. Condens. Matter* **13**, 8587 (2001).
- [29] M. Geilhufe, S. Achilles, M. A. Köbis, M. Arnold, I. Mertig, W. Hergert, and A. Ernst, *J. Phys. Condens. Matter* **27**, 435202 (2015).
- [30] E. M. Godfrin, *J. Phys. Condens. Matter* **3**, 7843 (1991).
- [31] Y. Takagi, K. Isami, I. Yamamoto, T. Nakagawa, and T. Yokoyama, *Phys. Rev. B* **81**, 035422 (2010).
- [32] Y. Takahashi, T. Miyamachi, K. Ienaga, N. Kawamura, A. Ernst, and F. Komori, *Phys. Rev. Lett.* **116**, 056802 (2016).
- [33] J. M. Gallego, D. O. Boerma, R. Miranda, and F. Ynduráin, *Phys. Rev. Lett.* **95**, 136102 (2005).
- [34] J. M. Gallego, S. Y. Grachev, M. C. G. Passeggi, F. Sacharowitz, D. Eciija, R. Miranda, and D. O. Boerma, *Phys. Rev. B* **69**, 121404 (2004).
- [35] C. Navio, J. Alvarez, M. J. Capitan, D. Eciija, J. M. Gallego, F. Ynduráin, and R. Miranda, *Phys. Rev. B* **75**, 125422 (2007).
- [36] T. Detzel and N. Memmel, *Phys. Rev. B* **49**, 5599 (1994).
- [37] N. Memmel and T. Detzel, *Surf. Sci.* **307**, 490 (1994).
- [38] J. Shen, J. Giergiel, A. Schmid, and J. Kirschner, *Surf. Sci.* **328**, 32 (1995).
- [39] G. Bayreuther, F. den Broeder, D. Chambliss, K. Johnson, R. Wilson, and S. Chiang, *J. Magn. Magn. Mater.* **121**, 1 (1993).
- [40] We checked the ionization of nitrogen molecules/atoms without bombardment using an ion gun. The ion flux monitored for the Fe evaporator increased in proportion to the rise in the N₂ pressure, far below the parameters at which Fe started to evaporate. This indicates the ionization of the N₂ molecules and/or N atoms around the evaporator, possibly by thermal electrons created inside it. Then, the N⁺ and N₂⁺ ions could reach the surface together with the evaporated Fe atoms, or iron nitride was already formed before landing.
- [41] The number of the Fe atoms detected in the edge-jump spectra was smaller than that expected from the initially deposited ones. This implies that a certain number of Fe atoms not participating in forming any γ' -Fe₄N structures were embedded in the Cu substrate during annealing, at least several nanometers (probing depth in the TEY mode) below the surface.
- [42] Y. Shi, Y. Du, and G. Chen, *Solid State Commun.* **152**, 1581 (2012).
- [43] See Ref. [32] for a detailed state assignment to the STS peaks observed in the monolayer γ' -Fe₄N.
- [44] P. Carra, B. T. Thole, M. Altarelli, and X. Wang, *Phys. Rev. Lett.* **70**, 694 (1993).
- [45] B. T. Thole, P. Carra, F. Sette, and G. van der Laan, *Phys. Rev. Lett.* **68**, 1943 (1992).
- [46] C. T. Chen, Y. U. Idzerda, H.-J. Lin, N. V. Smith, G. Meigs, E. Chaban, G. H. Ho, E. Pellegrin, and F. Sette, *Phys. Rev. Lett.* **75**, 152 (1995).
- [47] Y. B. Xu, E. T. M. Kernohan, D. J. Freeland, A. Ercole, M. Tselepi, and J. A. C. Bland, *Phys. Rev. B* **58**, 890 (1998).
- [48] The difference in the DOSs between (Fe1, Fe2) in the monolayer γ' -Fe₄N and (Fe1, Fe2) and (Fe5, Fe6) in the trilayer one is just a switch of the orbital assignment between d_{yz} and d_{zx} . Therefore, the DOSs of Fe2 in the monolayer γ' -Fe₄N and Fe2 and Fe6 in the trilayer one are not presented here.
- [49] J. Tersoff and L. M. Falicov, *Phys. Rev. B* **26**, 6186 (1982).
- [50] O. Hjortstam, J. Trygg, J. M. Wills, B. Johansson, and O. Eriksson, *Phys. Rev. B* **53**, 9204 (1996).
- [51] R. Nakajima, J. Stöhr, and Y. U. Idzerda, *Phys. Rev. B* **59**, 6421 (1999).
- [52] D. Pescia, M. Stampanoni, G. L. Bona, A. Vaterlaus, R. F. Willis, and F. Meier, *Phys. Rev. Lett.* **58**, 2126 (1987).
- [53] R. Lorenz and J. Hafner, *Phys. Rev. B* **54**, 15937 (1996).
- [54] P. Bruno, *Phys. Rev. B* **39**, 865 (1989).